

A *Chandra* View of the Anomalous *Half-Merger* NGC520

Andrew M. Read¹

¹ *Dept. of Physics and Astronomy, Leicester University, Leicester LE1 7RH, U.K.*
(E-mail: amr30@star.le.ac.uk)

Accepted; Received; in original form

ABSTRACT

High spatial and spectral resolution *Chandra* X-ray observations of the anomalous merging galaxy NGC520, a similarly-evolved system to the well-known Antennae galaxies, are presented here.

Of great interest is the fact that NGC520, on account of it being supposedly due (as seen in various multi-wavelength studies) to the result of an encounter between one gas-rich disk and one gas-poor disk, appears in X-rays to be only ‘half a merger’; Whereas a ULX lies at the primary (SE), more-massive nucleus, no sources are seen at the secondary nucleus. Whereas what appears to be a starburst-driven galactic wind is seen outflowing perpendicular to the molecular disk surrounding the primary nucleus, no such diffuse structure is seen anywhere near the secondary nucleus. Comparing the X-ray properties with those of other merging galaxies, including famous gas-rich–gas-rich mergers such as the Mice and the Antennae, one sees that, relative to its SFR, the number of ULXs seen within the system is rather small. Similarly the total X-ray luminosity and the fraction of this emission that appears diffuse are both a factor ~ 2 less than that expected based on NGC520’s evolutionary merger stage.

Though only half of NGC520 appears in X-rays as other mergers do, there is still a wealth of structure and detail; 15 X-ray sources are detected within the system, many of them showing long-term variability, including a small number of bright ULXs that flatten the source X-ray luminosity function to a level similar to that of the Antennae and other mergers. Lastly, to see what appears to be a starburst-driven diffuse galactic wind, with a spectrum entirely consistent with that of other known galactic winds, though unusually, emanating from only one of the nuclei, is a surprise, given that one might have expected such structures to have distorted very quickly in such a rapidly evolving environment. The wind is larger and more massive than structures seen in evolutionarily earlier systems (e.g. the Mice), but smaller and less massive than as seen in later systems (e.g. the Antennae), or classic starbursts. Perhaps these structures can survive for longer than was previously thought.

Key words: galaxies: individual: NGC520 – galaxies: starburst – galaxies: ISM – galaxies: halos – X-rays: galaxies – ISM: jets and outflows

1 INTRODUCTION

Merging and interacting are key elements in the life of galaxies, and underpin most current theories of galaxy formation and evolution. There are probably very few galaxies today that were not shaped by interactions or even out-right mergers. Many mergers appear luminous in all wavebands. A very intense ($L_{\text{bol}} > 10^{12} L_{\odot}$) and spatially extended burst of star formation occurs in the evolution of most mergers. Toomre’s (1977) hypothesis, whereby elliptical galaxies might be formed from the merger of two disk galaxies, is now generally accepted, such behaviour having been modelled in many N-body simulations of mergers (e.g.

Toomre & Toomre 1972; Barnes 1988). During such an encounter, the conversion of orbital to internal energy causes the two progenitor disks to sink together and coalesce violently into a centrally condensed system. The ‘Toomre sequence’ (Toomre 1977) represents probably the best examples of nearby ongoing mergers, from disk-disk systems to near-elliptical remnants.

NGC 520 (Arp 157), the ‘second brightest very disturbed galaxy in the sky’ (Arp 1987) lies seventh in the Toomre sequence, and is classified as an intermediate-stage merger by Hibbard & van Gorkom (1996), is as radio and infrared bright as the famous merging system the *Antennae*, and has two smaller tails as well as two nuclei and

two velocity systems in its spectra, indicative of a young merger. Some properties of the system are given in Table 1. A distance to NGC520 of 28 Mpc is assumed in this paper (Read & Ponman 1998 [hereafter RP98]; Tully 1988), hence $1'$ corresponds to ~ 8 kpc. A brief introduction to the system is given below, and the previous X-ray observations are described in Sec.1.1.

The nature of the peculiar system NGC 520 was once a puzzle; is it one disturbed galaxy or two interacting galaxies? Stanford and Balcells (1990) detected two galactic nuclei, just visible in the optical but more clearly in the K-band. The less massive, secondary component (by perhaps more than an order of magnitude) is the northwestern (NW) knot, which is optically brighter than the main (primary; SE) component. The main component is optically weak because it is seen edge-on, and the light from its central region is absorbed by interstellar dust in its disk (visible as a dark lane in Figure 1 of Bernlöhr 1993). Furthermore, two hypotheses, either that the nearby dwarf galaxy UGC 957 might be primarily responsible for the disturbed morphology of a single galaxy in NGC 520, or that two interacting disk systems formed NGC 520, were tested with numerical simulations (Stanford and Balcells 1991). The simulations indicate that NGC 520 contains two interacting disks which collided $\sim 3 \times 10^8$ years ago (UGC 957 was only involved in the producing of the northern half of a tidal tail).

Tovmasyan and Sramek (1976) found that the compact radio source in NGC 520 is situated in the dark lane between the two visible parts of the system. Condon et al. (1982) later resolved this into a $6''$ extension, consistent with an edge-on disk, lying almost east-west. More recent subarcsecond angular resolution observations of the neutral gas and of the radio continuum structure at 1.4 and 1.6 GHz (Beswick et al. 2003) show this $6''$ feature to be made up of $\sim 10 - 15$ individual clumps. Further, none of the clumps are found to have a radio spectral index compatible with AGN, and hence the most probable source of the radio emission is a nuclear starburst.

Millimetre-wave interferometer maps of the $2.6\mu\text{m}$ CO emission (Sanders et al. 1988) show a strong peak at the position of this radio source; approximately $1.9 \times 10^9 M_\odot$ of molecular gas is concentrated in a region approximately 0.8 kpc in size. More recently, Yun & Hibbard have mapped the CO $J = 1 \rightarrow 0$ emission, and this is seen to form an east-west ring-like structure coincident with the radio structure. No molecular gas is seen near the NW nucleus, or indeed elsewhere in the system, and Yun & Hibbard suggest that the progenitor disk surrounding the secondary nucleus was rather gas-poor.

Much of the extranuclear regions of both galaxies within NGC 520 experienced a period of enhanced star formation $\sim 3 \times 10^8$ years ago. The main sequence remnants of this burst are the A stars whose features are evident in the optical spectra (Stanford 1991). The putative burst within the less massive NW nucleus has returned to a nominal level. The more massive, optically hidden SE nucleus produces stars at a rate of $\sim 0.7 M_\odot \text{ yr}^{-1}$ and is the current dominant source of star formation in this system. The star formation rate within this region is ~ 35 times higher than for an isolated disk galaxy. This region dominates the mid-infrared flux of the system, and probably produces most of the far-infrared flux seen in NGC 520.

The X-ray observations of NGC520 prior to Chandra are described in the following subsection. Section 2 describes the Chandra observations and the data reduction techniques used. Discussion of the spatial, spectral and temporal properties of the source and diffuse emission components follow in Section 3, and in Section 4, the conclusions are presented.

1.1 Previous X-ray Observations

NGC520 has only previously been observed in X-rays with ROSAT, and the PSPC and HRI data were presented in RP98. The one PSPC source detected in the vicinity of NGC 520 at $\alpha = 01h24m34.76s$, $\delta = +03d47m39.7s$, lies within $\sim 5''$ of the radio source resolved by Condon et al. (1982), and is coincident with the more massive (the SE) of the two nuclei, as visible in the K-band image of Stanford & Balcells (1990). No source was detected at the position of the secondary NW nucleus.

NGC 520 appeared to be a very compact X-ray source with, very unusually for this type of system, and considering how infrared bright it is, little in the way of diffuse emission – a comparison of the radial emission profile with the ROSAT PSPC PSF indicated very little emission beyond $0.6'$. The PSPC emission is almost consistent with point source emission, and what diffuse emission exists, only makes up a very small fraction of the total. Little could be said about the spectral properties of the diffuse emission, except that it appeared soft.

The HRI image (RP98) showed more detail, and three sources were detected, the most northerly centred less than $5''$ east of the secondary (optically brighter) nucleus. This source, apparently associated with the NW nucleus, appears to be the hardest of the sources. A suggested extension to the east was also observed. The two other HRI sources both appear to be soft and they follow the bright band of optical emission down the north-eastern side of the system.

2 CHANDRA OBSERVATIONS, DATA REDUCTION AND RESULTS

NGC520 was observed with Chandra on January 29th, 2003 for a total of just over 41 ks, with the back-illuminated ACIS-S3 CCD chip at the focus (Observation ID: 2924). Data products, correcting for the motion of the spacecraft and applying instrument calibrations, were produced using the Standard Data Processing (SDP) system at the Chandra X-ray Center (CXC). These products were then analysed using the CXC CIAO software suite (version 3.0).

A lightcurve extracted from a large area over the entire observation was seen to be essentially constant and consistent with a low-level rate, apart from a couple of high-background peaks. Screening of the data to remove these periods (at a level of $2.44 \text{ ct s}^{-1} \text{ arcmin}^{-2}$) was performed.

2.1 Overall X-ray structure

Fig.1 (left) shows contours of adaptively smoothed (0.2–10 keV) Chandra ACIS-S X-ray emission from the field surrounding NGC520, superimposed on the V-band KPNO 0.9 m image from Hibbard & van Gorkom (1996). Note that the secondary (NW), less-massive nucleus is quite visible in

System	Other names	Distance (Mpc)	$\log L_B$ (erg s^{-1})	$\log L_{FIR}$ (erg s^{-1})	L_{FIR}/L_B	S_{60}/S_{100}	$\log L_{rad}$ W Hz^{-1}
NGC 520	Arp 157	28	43.87	44.15	1.900	0.651	22.24

Table 1. Selected properties of NGC520. Distance and optical luminosity L_B are taken from Tully (1988). FIR luminosity is calculated from IRAS 60 and 100 μm fluxes, S_{60} & S_{100} , (taken from the IRAS Point Source Catalogue), using the expression $L_{FIR} = 3.65 \times 10^5 [2.58S_{60\mu\text{m}} + S_{100\mu\text{m}}] D^2 L_\odot$ (e.g. Devereux & Eales 1989). Radio luminosity is taken from Condon et al. 1990.

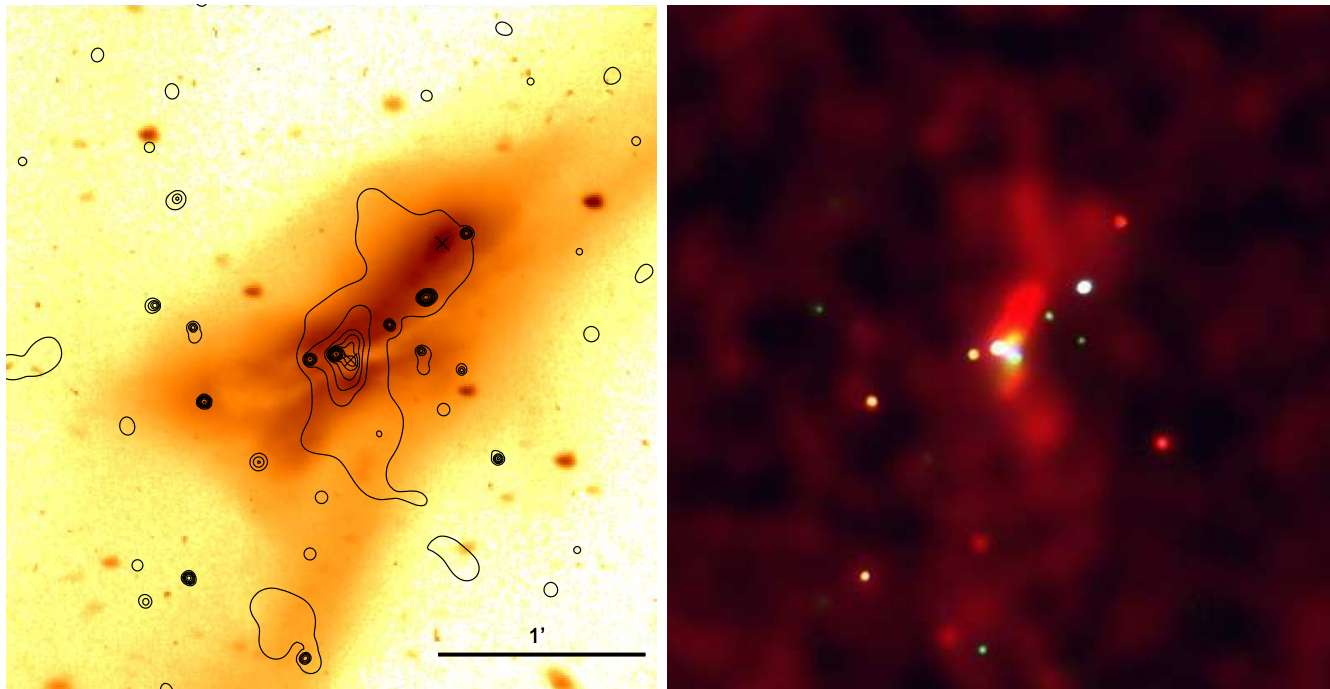


Figure 1. (Left) Contours of adaptively-smoothed (0.2–10 keV) Chandra ACIS-S X-ray emission from the field surrounding NGC520, superimposed on the V-band KPNO 0.9 m image from Hibbard & van Gorkom (1996). The X-ray contours increase by factors of two. The crosses mark the positions of the two nuclei (from Stanford (1991)). (Right) ‘True colour’ X-ray image of NGC520 to the same scale. Red corresponds to 0.2–0.9 keV, green to 0.9–2.5 keV and blue to 2.5–10 keV. For scale, the images are approximately 3’ to a side.

the optical image, whereas the primary (SE) nucleus is hidden by the obscuring dust lane. The adaptive smoothing of the X-ray emission attempts to adjust the smoothing kernel to obtain a constant signal-to-noise ratio across the image.

Several things are immediately evident from the image. Many bright point sources are visible within the optical confines of the system. Residual, perhaps diffuse emission is seen concentrated and centred in the dust lane at the centre of the galaxy, but extending initially in a general north-south direction, and also following slightly the general shape of the galaxy to the north-west.

Fig. 1 (right) shows a true colour X-ray image, with red corresponding to 0.2–0.9 keV, green to 0.9–2.5 keV and blue to 2.5–10 keV. The individual adaptively-smoothed images were obtained as described above. The image is to the same scale as Fig. 1 (left), and all the X-ray features are visible. A large range in spectral hardness is seen within the point sources, and the residual, perhaps diffuse emission is seen to be very much softer than the point source emission.

2.2 Point sources: spatial and spectral properties

The CIAO tool *wavdetect* was used to search for point-like sources, on scales from 1–16 pixels (0.5–8’). A total of 15 sources were detected in the 0.2–7.5 keV band within or close to the optical confines of the galaxies, and their X-ray properties are summarised in Table 2. Fig. 2 shows the positions of the detected sources.

The X-ray properties given in Table 2 are as follows; Right Ascension and Declination (2000.0) are given in cols. 2 and 3, together with (col. 4) the positional error (in arcseconds), calculated from from the *wavdetect* errors in RA and Dec (no corrections on the absolute astrometry have been applied). Net source counts (plus errors, both from CIAO-*wavdetect*) are given in col. 5, and the source significance is given in col. 6. Cols. 7 and 8 give the fitted hydrogen column and power law photon index (an ‘F’ indicating that the parameter was frozen (see below for a discussion of the spectral fitting)). For those fits where a significant number of degrees of freedom existed (> 1 ; see below), this is given, together with the best fit χ^2 in col. 9. Finally, (0.2–10 keV)

Table 2. Sources detected by *wavdetect* in the 0.2–7.5 keV band within or close to the optical confines of NGC520. Columns are described in the text. Luminosities assume a $\Gamma = 1.5$ photon index power law plus Galactic absorption, except for sources 9, 11, 12 and 15, where the spectral parameters are given. A distance of 28 Mpc has also been assumed.

Src.	RA (2000.0)	Dec.	Pos.err. (arcsec)	Counts(err)	Sig.	N_{H} 10^{20} cm^{-2}	Photon Index Γ	χ^2 (N_{dof})	L_X (0.2–10 keV) ($10^{39} \text{ erg s}^{-1}$) (emitted) (intrinsic)	
7	01 24 37.82	+03 46 25.9	0.11	34.7± 6.0	14.2	3.27(F)	1.5(F)	-	0.75	0.77
8	01 24 37.67	+03 47 16.1	0.08	48.2± 7.1	18.5	3.27(F)	1.5(F)	-	0.92	0.95
9	01 24 35.68	+03 47 29.7	0.14	56.0± 8.0	14.1	$108^{+77.8}_{-22.9}$	$3.5^{+0.6}_{-0.8}$	2.7(3)	0.80	4.38
10	01 24 35.50	+03 46 04.9	0.22	22.4± 5.0	7.9	3.27(F)	1.5(F)	-	0.74	0.75
11	01 24 35.19	+03 47 31.4	0.24	874.9±30.5	103.2	$40.0^{+3.9}_{-3.5}$	$2.4^{+0.1}_{-0.1}$	74.5(73)	15.89	34.97
12	01 24 34.89	+03 47 29.5	0.13	111.6±13.2	12.5	$48.4^{+45.0}_{-21.3}$	$1.1^{+0.4}_{-0.2}$	40.4(20)	8.89	10.13
13	01 24 34.19	+03 47 40.4	0.23	21.9± 5.1	6.8	3.27(F)	1.5(F)	-	0.60	0.61
14	01 24 33.53	+03 47 33.4	0.32	11.9± 3.7	4.4	3.27(F)	1.5(F)	-	0.23	0.25
15	01 24 33.50	+03 47 48.8	0.05	354.0±19.2	75.1	$44.5^{+13.7}_{-9.9}$	$1.8^{+0.1}_{-0.1}$	23.1(30)	10.00	13.45
18	01 24 32.79	+03 48 07.4	0.16	21.0± 4.8	7.8	3.27(F)	1.5(F)	-	0.29	0.30
19	01 24 32.73	+03 47 29.1	0.35	8.8± 3.2	3.6	3.27(F)	1.5(F)	-	0.21	0.22
20	01 24 31.96	+03 47 04.4	0.28	15.1± 4.2	5.2	3.27(F)	1.5(F)	-	0.36	0.36
23	01 24 40.23	+03 45 50.0	0.35	12.0± 3.9	4.1	3.27(F)	1.5(F)	-	0.17	0.17
25	01 24 37.99	+03 47 36.9	0.32	9.2± 3.3	3.5	3.27(F)	1.5(F)	-	0.34	0.34
26	01 24 36.60	+03 46 59.9	0.31	8.0± 3.0	3.4	3.27(F)	1.5(F)	-	0.20	0.22

X-ray emitted and intrinsic (i.e. corrected for absorption) luminosities are given in cols. 10 and 11.

Source spectra were extracted at the exact positions given by the 0.2–7.5 keV detection analysis. The regions output by the detection routines were invariably near-circles of radius $\lesssim 8$ pixels (partly due to NGC520 only occupying the very centre of the ACIS-S3 chip). Consequently a single extraction radius of 8 pixels ($4''$) was defined and used for all the sources in Table 1. A large area to the SW of the system, chosen close enough to the system to minimise effects related to the spatial variations of the CCD response, but free of source and apparent diffuse emission, was chosen to construct a background spectrum.

ACIS spectra were extracted using Pulse Invariant (PI) data values, and were binned together to give a minimum of 10 counts per bin after background subtraction. Hence χ^2 statistics could be used. Response matrices and ancillary response matrices were created for each spectrum, using the latest calibration files available at the time of writing.

Standard spectral models were fit to the spectral data using the XSPEC spectral fitting software. Events above 7.5 keV (of which there were very few) and below 0.25 keV were excluded from the fitting on the grounds of uncertainties in the energy calibration. It is now known that there has been a continuous degradation in the ACIS QE since launch. A number of methods now exist within the community to correct for this. These include the release of an XSPEC model (ACISABS) to account for this degradation, and the existence of software (corrarf) to correct the ancillary response files. The analysis performed in the present paper has made use of CALDB v2.23, which does not include a correction for the ACIS QE degradation. Hence, both the above methods have been used here in the spectral fitting, and very similar results were obtained. In both cases, the time since launch of the observations (here, 1286 days) is used in the correction. Although the calibration at energies below 1.0 keV is believed to be uncertain, data in this range were kept, as the statistical error on these data points is

still greater than the errors due to the uncertainties in the calibration.

Two models, one incorporating absorption fixed at the value out of our Galaxy ($3.27 \times 10^{20} \text{ cm}^{-2}$) and a 5 keV *mekal* thermal plasma, the other incorporating absorption (again, fixed) and a power-law of photon index 1.5 were fit to the source data. For the majority of the sources, there were insufficient counts to allow the model parameters to vary, but for sources 9, 11, 12 and 15, there were sufficient counts (>50) to allow the model parameters to fit freely.

For 3 of these 4 cases (9, 11 and 15), F-tests showed that statistically significant improvements in the fits were made on freeing the parameters. Also in these 3 cases, better fits (with reduced $\chi^2 \lesssim 1$) were obtained using a power-law model over a thermal model, and these model parameters are quoted in Table 2. The fit to source 12 is not too good (with a reduced χ^2 of ≈ 2), and this is discussed further in Section 3.1.

The luminosities quoted in Table 2 for sources 9, 11, 12 and 15 assume these best-fit models, while for the other sources, the model assumed is of a fixed (Galactic) absorption plus a power-law of photon index 1.5.

2.3 Residual emission: spatial and spectral properties

The existence of residual, likely diffuse emission is very evident in the figures. A spectrum from this region of apparent diffuse emission was extracted – the ellipse in Fig. 3 shows the area over which the spectrum was extracted, with the sources also excluded to a radius of $4''$. Again the spectral channels were binned together to give a minimum of 10 counts per bin.

The spectral fitting was performed as for the point sources, using the same models, and using both methods to correct for the degradation in the ACIS QE. While an absorption plus power-law model was unable to fit the data satisfactorily, a thermal model proved much better, and the

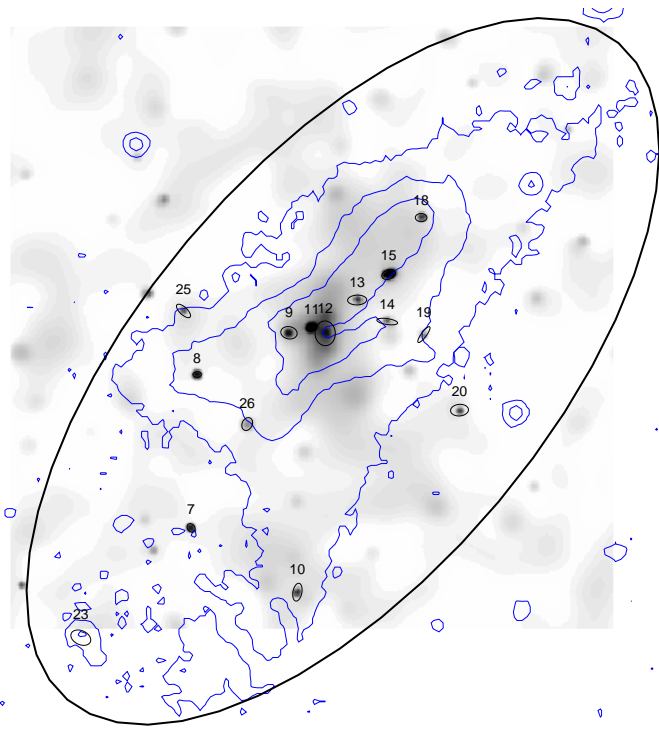


Figure 2. Adaptively-smoothed (0.2–10 keV) ACIS-S image labelled with sources detected in the 0.2–7.5 keV band. The large ellipse shows the area over which the diffuse emission spectrum was extracted, and the blue contours show schematically the optical confines of the system (see Fig. 1).

best thermal fit (using an absorption plus *mekal* model) is summarised in Table 3; the absorbing column, the fitted temperature and metallicity, the reduced χ^2 , and the emitted and intrinsic (i.e. total N_H absorption-corrected) X-ray luminosity is given. The data plus best fit model is shown in Fig. 3. A re-analysis of the data using a grouping of 20 counts per bin gave essentially identical results to those given here.

3 DISCUSSION

3.1 Point sources

Within the general optical confines of NGC520 (i.e. within the ellipse shown in Fig. 2), 15 sources are detected with the Chandra ACIS-S instrument, down to a (0.2–10.0 keV) detection limit of $\approx 1.7 \times 10^{38}$ erg s $^{-1}$. Previous detections of X-ray sources include the one source (P1) detected with the ROSAT PSPC, and the three sources (H1–H3) detected by the ROSAT HRI (RP98). One can use the the logN–logS relations of Rosati et al. (2002) to estimate the expected number of background sources not physically associated with NGC520. At most, perhaps 2 background sources are expected over the ellipse covered by Fig. 2 at the detection limit seen here.

Source 12 is bright (though only the third brightest source), spectrally quite hard (as indicated by the blue-white appearance in the RGB plot - Fig. 1 [right]), and is coincident ($< 0.5''$) with the primary nucleus, i.e. the Condon et al. (1982) radio source and the Yun & Hibbard (2001) CO

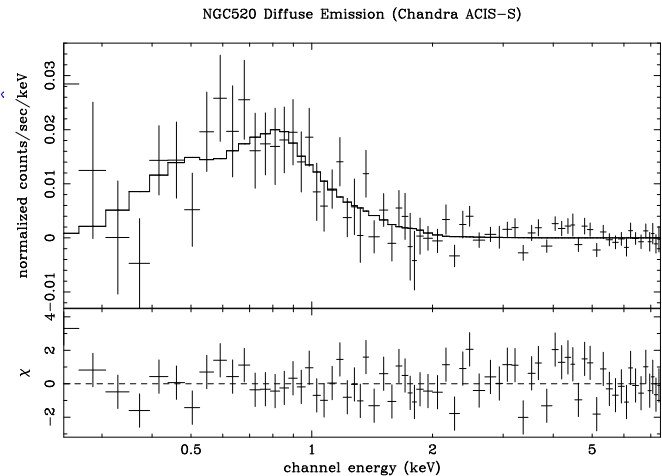


Figure 3. Data (points) plus best-fit thermal mekal model (lines) for the residual emission within NGC520. The lower panel shows the (data–model) $\Delta\chi^2$ values.

feature. It lies at the centre of the brightest part of the much softer diffuse X-ray emission (discussed in the next subsection). The central region of NGC520 is shown more clearly in Fig. 4, where the adaptively-smoothed (0.2–10 keV) Chandra ACIS-S X-ray emission (from Fig. 1 [left]), the velocity-integrated CO(1–0) map of Yun & Hibbard (2001), the H α emission from Yun & Hibbard (2001), the Stanford (1991) primary nucleus position, the Condon et al. (1982) 6'' radio source and the positions of the main 1.4 GHz components resolved within the 6'' Condon feature by Beswick et al. (2003) are all shown together. In actuality, Chandra source 12 lies closest to ($< 0.2''$) the brightest and central-most of the Beswick et al. (2003) radio features – their feature 6. Taking also into account uncertainties in Chandra’s absolute astrometry ($\approx 0.7''$ for on-axis, isolated point sources), then the Chandra source 12 error circle could also just encompass radio feature 7 (the 2nd brightest feature of Beswick et al. 2003). Chandra source 12 is undoubtedly associated with the primary nucleus of NGC520. A spectral fit to source 12’s spectrum, but using a model incorporating an extra component to represent the soft, thermal diffuse emission (with fixed parameters as given in Table 3), results in a far better fit to the source 12 data (with a reduction in reduced χ^2 of $\gtrsim 0.5$). An F-test shows this improvement to be statistically significant at over 97% confidence. Here, the hard component (assumed due to the actual source 12 itself) is better represented by a power-law model ($N_H=2.3 \times 10^{22}$ cm $^{-2}$, $\Gamma=2.15$) than a thermal model ($N_H=2.5 \times 10^{22}$ cm $^{-2}$, $kT=3.1$ keV). In both cases, the hard (i.e. the point source) component makes up $\approx 90\%$ of the total emitted (0.2–10 keV) flux from source 12.

Source 11 is the brightest of the X-ray sources and lies at the easternmost edge of the radio/CO disk. Though it could be enclosed within the ROSAT H3 and H2/P1 sources and the complex and confused PSPC/HRI emission surrounding the primary nucleus, this appears not too likely. Source 15, the second brightest source, does not have a direct counterpart in the HRI (or the relatively poor positional resolution PSPC) observations, and this would indicate that source 15

Table 3. Best results of fitting a thermal model to the spectrum of the residual emission within NGC520. Luminosities assume a distance of 28 Mpc (see text).

Diff. Src.	Counts(err)	N_{H} (10^{20} cm^{-2})	kT (keV)	Z (solar)	χ^2 (red.)	L_X (0.2–10 keV) ($10^{39} \text{ erg s}^{-1}$) (emitted) (intrinsic)
NGC520	896.8±112.6	3.27(F)	0.58 $^{+0.09}_{-0.11}$	< 0.04	0.95	6.40 8.03

(and likely source 11) are transient in nature. Both sources are well fit with single component power-law models (Table 2).

Sources 8 and 9 are both fairly bright and fairly soft/medium-temperature sources. Source 9 is associated with H3, and source 8 may have a low-significance HRI counterpart. Of the remaining, lower-luminosity sources, source 18 lies closest to the secondary (NW) nucleus (visible in the V-band image of Fig. 1 [left]), but still lies some 7'' distant – hence, interestingly, no X-ray emission is coincident with the secondary nucleus, and the HRI source (H1) tentatively associated (RP98) with the NW nucleus appears to have vanished. Given the astrometric uncertainties in the *ROSAT* position it is unlikely that source 8 is coincident with H1.

Beswick et al. (2003) believe that two different components of gas (neutral gas and ionised gas), with very different velocity characteristics, can be sampled within NGC520, and these components are located at different distances from the primary nucleus. Whereas the velocity structure of the neutral ISM components within the central regions of the primary nucleus (Fig. 4) are probably more characteristic of the rotational motion of the progenitor galaxy nucleus, the very different velocities observed (e.g. Stockton & Bertola 1980; Bernlöhr 1993) for the ionised gas located a few kpc from the primary nucleus have likely been imparted on the gas by the merger event. It is very interesting to note that there are many bright sources (notably 9, 11 & 13) that lie in this zone where the two velocity systems are colliding, a region where strong shocks and large compressions of gas are expected to occur. Indeed, the H α emission (Yun & Hibbard 2001) indicates that a good deal of star-formation is certainly taking place on the eastern side of the zone where the two velocity systems are colliding, in the region occupied by sources 9 and 11.

The cumulative X-ray luminosity function (XLF) of the sources detected within NGC520 is shown in Fig. 5. Plotted is the (log of the) number of sources above a given X-ray luminosity versus (log of the) X-ray luminosity. The functions for the intrinsic and emitted values (see Table 2) are given. While simple regression fitting of a linear function to $\log N$ against $\log L_X$ leads to a slope of 0.45 (usage of the emitted L_X values leads to a slope of 0.50), a more appropriate approach, and one where the errors of the Poissonian statistics of the data are better reflected, is to fit the differential luminosity function, using the method of Crawford et al. (1970). This gives more realistic errors on the fitted slope. Usage of this method gives slopes of 0.58 ± 0.15 for the intrinsic L_X values (and 0.66 ± 0.17 for the emitted L_X values).

Colbert et al. (2003) have found that, while ellipticals have very steep XLF slopes (-1.41 ± 0.38), the slopes for spirals are much flatter (-0.79 ± 0.24), and for merging galax-

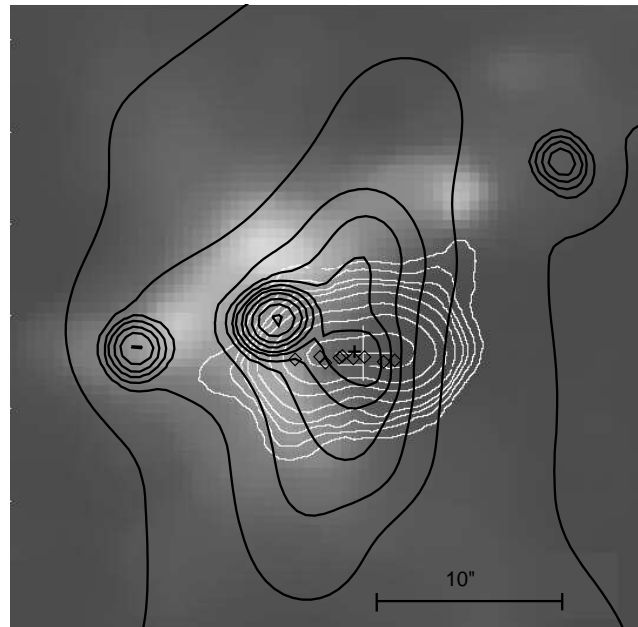


Figure 4. The central region of NGC520: Black contours show the contours of adaptively-smoothed (0.2–10 keV) Chandra ACIS-S X-ray emission (from Fig. 1 [left]). White contours show the velocity-integrated CO(1–0) map of Yun & Hibbard (2001). The small black cross shows the position of the primary nucleus from Stanford (1991). The large white cross shows the centre of the 6'' radio source of Condon et al. (1982), and the diamonds show the positions of the nine main 1.4 GHz components resolved within the 6'' Condon feature by Beswick et al. (2003). The underlying grey-scale shows the H α image emission from Yun & Hibbard (2001). The image is $\approx 33''$ across.

ies and irregular galaxies, the slope is even flatter still (-0.65 ± 0.16). NGC520 therefore has a very flat XLF, consistent with it being a highly irregular, merging galaxy. NGC520 in fact has an XLF slope similar to that of the *Antennae* (-0.47 ± 0.05 ; Zezas & Fabbiano 2002), a system with a very similar far-infrared luminosity, and a system at a similar to slightly later evolutionary stage.

The number of Ultraluminous X-ray Sources (ULXs), i.e. sources with $L_X \gtrsim 10^{39} \text{ erg s}^{-1}$, in NGC520 is around 3–4 (i.e. sources 11, 12 and 15, with possibly source 9). Were it not for these sources, the XLF would appear rather steeper than it does in Fig. 5, looking more like that of normal spirals. The 3 definite ULXs in fact, make up most of total X-ray flux, accounting for 85% of the point source emission, and 73% of the total emission.

There is evidence to suggest that galaxies with a greater

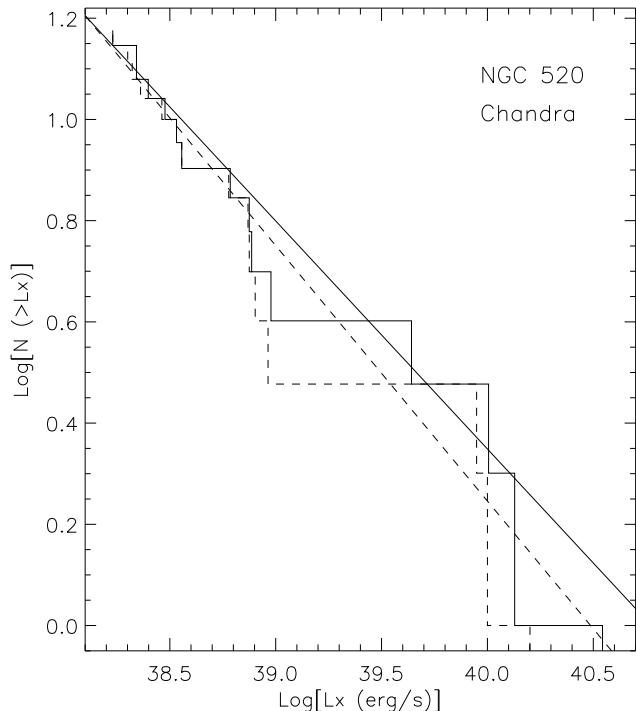


Figure 5. The cumulative luminosity function of the discrete sources detected within NGC520. Plotted is the log of the number of sources above a given X-ray luminosity versus (log of the) X-ray luminosity. The functions for the intrinsic (solid line) and emitted (dashed line) values (see Table 2) are given. The straight solid and dashed lines show the best regression fits to the two functions (see text).

star formation rate contain a greater number of ULX’s (Swartz et al. 2004), and it is these sources that flatten the XLF. Brassington et al. (2004) have presented a relationship between the number of ULXs and the far-infrared luminosity for a small number of interacting and merging galaxies: $\log N(\text{ULX}) \propto \log L_{\text{FIR}}^{0.18 \pm 0.13}$. NGC520 appears unusual in that it does not fit into this picture at all, having a large L_{FIR} value, very like that of e.g. the *Mice* or the *Antennae*, but a relatively small number of ULXs (3–4). One would expect, based on the number of ULXs per unit far-infrared luminosity, there to be about 10 ULXs in NGC520, if it were similar to the *Antennae*.

Furthermore, Brassington et al. (2004) observe a relationship between the integrated luminosity of the ULX sources and the far-infrared luminosity in their merging galaxy sample: $\log L_{\text{ULX}} \propto \log L_{\text{FIR}}^{0.54 \pm 0.04}$. The small number of NGC520 ULXs are all bright, but even so, NGC520 lies significantly below the observed $L_{\text{ULX}} - L_{\text{FIR}}$ relationship.

3.2 Diffuse emission

The residual emission, given its structure and its spectrally soft, single-component nature, is very likely predominantly due to genuinely diffuse hot (0.58 keV) gas (though there will be some contribution from unresolved sources).

It appears centred on Chandra source 12, at the precise site of the primary, more massive, optically-obscured

nucleus, a nucleus believed not to harbour any AGN, but believed to be a starburst-powered nucleus (Beswick et al. 2003). The diffuse emission is seen to extend in a bipolar form initially to the north and to the south, i.e. directly perpendicular to the molecular disk (Yun & Hibbard 2001) surrounding the primary nucleus, a disk also observed in the radio (Condon et al. 1982; Beswick et al. 2003). This north-south extension is seen to be quite bright for quite a distance (~ 2 kpc from the nucleus), and then becomes somewhat weaker, perhaps more so to the south, reaching a final extent of perhaps ~ 7 kpc (to the north) and ~ 5.5 kpc (to the south). It is quite unlikely that the north-south extension could be predominantly due to absorption by cold disk gas, as the CO gas exists in only a small ($\sim 12''$) centralised region, and the rather diffuse neutral HI gas (Yun & Hibbard 2001) pervades much of the system, and extends in a more SE-NW direction, in a direction roughly connecting the two nuclei. It is very interesting to note that there appears to be no significant enhancement in the diffuse emission, nor in the X-ray emission in general, in the vicinity of the secondary nucleus.

All these points, both spatial and spectral, are very suggestive of the diffuse structure being due predominantly to a small version of a starburst-driven wind from solely the primary (SE) nucleus. Further evidence is suggested by the ionised $\text{H}\alpha$ emission (visible in Fig. 4), following roughly the inner structure of the diffuse X-ray feature. Yun & Hibbard (2001) conclude that this $\text{H}\alpha$ emission is likely dominated by the ‘starburst-driven ionised wind’ escaping to the north and south. Interestingly, there is no evidence whatsoever for any similar structure in the secondary (NW) nucleus. Classic winds, such as those seen in famous nearby starburst galaxies such as M82 and NGC253 (e.g. Stevens, Read & Bravo-Guerrero 2002; Strickland et al. 2002) are rather isolated, and to see what appears to be a bipolar wind in even one member of a strong, rapidly-evolving interacting pair such as here in NGC520, is rather surprising. It is believed (Read 2003) that the very beginning of starburst-driven hot gaseous outflows in full-blown disk-disk mergers has been seen in the *Mice*. One might have thought that later systems would have evolved to such a degree, that any classic starburst wind or winds (were they to have existed), would have been distorted out of recognition, and indeed, Chandra observations of the *Antennae* (a system believed to be post-*Mice*, but more like at the evolutionary stage of NGC520) show a great deal of hot diffuse gas, but it has become all-pervasive, extending beyond the stellar bodies of the galaxies (Fabbiano et al. 2002).

One can infer mean physical properties of the hot gas around the northern and southern galaxies once some assumptions have been made regarding the geometry of the diffuse emission. Two models have been used here. A conservative model assumes the gas here to be contained in an elliptical bubble (the ellipse as shown in Fig. 2 and the third [line-of-sight] axis assumed equal [‘radius’ 9.2 kpc] to the short axis of the ellipse). A more stringent, and probably more realistic model roughly follows the outer contours of the X-ray emission and assumes the gas to be contained in a spherical bubble of radius $45''$ (corresponding to 6.1 kpc). Using these volumes, the fitted emission measure $\eta n_e^2 V$ (where η is the ‘filling factor’ - the fraction of the total volume V which is occupied by the emitting gas) can

be used to infer the mean electron density n_e , and hence, assuming a plasma composition of hydrogen ions and electrons, the total mass M_{gas} and thermal energy of the gas E_{th} . Approximate values of the cooling time t_{cool} of the hot gas, and also the mass cooling rate \dot{M}_{cool} can also be calculated. The resulting gas parameters for both models are listed in Table 4.

Comparing the diffuse gas parameters in Table 4 with those for isolated normal and starburst galaxies (Read, Ponman & Strickland 1997), and for merging galaxies (RP98; Fabbiano et al. 2002; Read 2003), one can say that the single diffuse outflow observed in NGC520 is larger than the outflows seen in the earlier-stage *Mice* (2 – 3 kpc), but is not as large as the classic winds of M82 and NGC253 (9–14 kpc), nor quite as large as the outflowing, non-collimated turbulent ISM of the Antennae (≈ 8 kpc). There appears to be more diffuse gas within the NGC520 system than in the *Mice*, but this gas mass, while possibly comparable to that of NGC253 and of order a half that seen in M82, is only 10-20% of that seen in the *Antennae*.

The injection rate of mechanical energy, or power injected into a particular galaxy by supernovae, can be estimated by the method employed in Read & Ponman (1995), and this value for NGC520 is seen to be very similar to that of the *Antennae* and M82. The amount of hot gas in NGC520, expressed as a fraction of input energy therefore, is rather small. Note that, as the diffuse gas has a very long cooling time, no significant fraction of the gas has had time to cool.

Though it is believed that the hot ISM of starburst galaxies has a multi-temperature structure, the single temperature obtained from the spectral fitting of the diffuse spectrum (≈ 0.58 keV) is entirely consistent with the range obtained for other starburst and merging galaxies.

3.3 X-ray emission from NGC520

NGC520 is very far-infrared bright, and consequently has a large value of L_{FIR}/L_B . It also has a large far-infrared temperature, S_{60}/S_{100} , and both these are indicative of NGC520 having a high SFR and being very active, more active than the famous interacting systems The *Mice* and The *Antennae*.

The total emitted 0.2–10 keV X-ray luminosity of NGC520, assuming a distance of 28 Mpc is 4.74×10^{40} erg s^{-1} , of which the diffuse emission makes up 13.5% (the equivalent intrinsic absorption-corrected values are 7.64×10^{40} erg s^{-1} and $f_{\text{diff}} = 10.5\%$).

The value of L_X quoted here may initially appear at odds with the low value ($\approx 1 \times 10^{40}$ erg s^{-1}) given in RP98. There are a few points here to note: The energy bands over which the luminosities are calculated are different. The RP98 value is based on the results of spectrally fitting the PSPC data, and this analysis was prone to difficulties and the spectral parameters obtained had large errors. In actuality, using PIMMS to predict the Chandra ACIS-S count rate, based purely on the HRI count-rate, allowing for the different energy ranges, and using a much more appropriate spectral model (a $\Gamma = 1.5$ power-law) does give a similar result to what we actually observe with the ACIS-S (to within 2%). Lastly, there is quite evidently a lot of variability go-

ing on within the point sources, so we should expect some variation in L_X between the observations.

As such, the larger X-ray luminosity inferred here for NGC520, indicates that it is not as anomalous as was first thought in RP98 – both its position in the L_X-L_{FIR} plane (RP98 Fig. 14) and its position in the L_X/L_B -versus-age plane (RP98 Fig. 13) appear closer in line with the other similar-stage mergers than as depicted in RP98. However, while taking into account the points raised in the previous paragraph, NGC520 still appears somewhat underluminous in X-rays, for its merger stage, perhaps by a factor of up to 2.

Yun & Hibbard (2001) discovered that, though a dense concentration of molecular gas is seen at the primary (SE) nucleus, none is seen at the secondary (NW) nucleus, nor along the region bridging the two nuclei. Hibbard & van Gorkom’s (1996) analysis of the stellar and H I features in NGC520 indicated that NGC520 is the product of an encounter between a gas-rich disk and a gas-poor disk (e.g. an S0 and Sa galaxy). The absence here of molecular gas in the NW nucleus can be explained if little molecular gas had been compressed towards the nucleus during the merger process, there being little gas in the progenitor disk to start with. Similar analyses have concluded that systems such as the *Mice* and the *Antennae* are each the product of encounters between two gas-rich systems.

This initial lack of gas in the NW progenitor is a very likely explanation of several facets of the X-ray emission discussed here. That there was no gas in the disk meant that no gas could be funnelled towards the NW nucleus during the interaction. Consequently, little in the way of a starburst could take place at the NW nucleus, and no collections of supernovae could collect and expand outwards in the form of a starburst-driven wind or of fountains or chimneys etc. – there would be, as is observed, no diffuse X-ray emission surrounding the NW nucleus. The percentage of the total X-ray emission in NGC520 observed to be diffuse (f_{diff}) is low ($\sim 13.5\%$), when compared with roughly similar stage systems (e.g. the Antennae [45%]; Fabbiano et al. 2002), and even when compared with very early-stage interacting systems (e.g. Arp270 [29%]; Brassington et al. 2004). Were the progenitor disk that formed the NW nucleus initially gas-rich, then f_{diff} for NGC520 would certainly be larger (though not by a factor of two), and perhaps more in line with other merging systems.

Further, as discussed earlier, the number of ULXs observed is very low when compared to other mergers. It is well known (e.g. Roberts et al. 2002) that ULXs are more prevalent in regions of enhanced star-formation. If a starburst were to have occurred in the NW nucleus similar to that in the SE nucleus, then the number of ULXs within the NGC520 system may well have been more like that of similar merger systems.

Lastly, the arguments raised here could increase the total X-ray luminosity, perhaps by the factor of ~ 2 required, bringing NGC520 more in-line with its expected position in the X-ray evolution of merging galaxies.

Diff. Model	kT (keV)	r (kpc)	n_e (cm^{-3}) ($\times 1/\sqrt{\eta}$)	M_{gas} (M_{\odot}) ($\times \sqrt{\eta}$)	E_{th} (erg) ($\times \sqrt{\eta}$)	t_{cool} (Myr) ($\times \sqrt{\eta}$)	\dot{M}_{cool} ($M_{\odot} \text{ yr}^{-1}$)
Large Ellipse	0.58	9.2	6.9×10^{-3}	7.1×10^8	1.9×10^{57}	7590	0.094
Small Bubble	0.58	6.1	1.9×10^{-2}	2.8×10^8	7.6×10^{56}	3560	0.079

Table 4. Values of physical parameters for the diffuse gas associated with NGC520. The values quoted are for a large ellipsoidal bubble model and a small spherical bubble model (see text). η is the filling factor of the gas.

4 CONCLUSIONS

Presented here are high spatial and spectral resolution Chandra ACIS-S X-ray observations of the interacting galaxy system, NGC520, a system at a similar or slightly later evolutionary stage as the *Antennae*, i.e. more evolved than the *Mice* but not as evolved as the ultraluminous contact mergers, such as Arp220. The primary results can be summarised as follows:

- What appears to possibly be a starburst-driven galactic wind has been discovered, outflowing perpendicular to the molecular disk surrounding the primary, optically-obscured SE nucleus. No such structure, nor any significant diffuse feature of any kind is visible elsewhere in the system, and is notably absent from around the secondary NW nucleus. Fitting of this diffuse emission yields a temperature entirely consistent with well-known nearby galactic winds. In terms of extent and mass, the wind appears larger and more massive than the winds of earlier-stage mergers, but is only at most of order the size and mass of the winds seen in the smaller nearby starbursts, and is rather much smaller and less massive than the diffuse structure seen in e.g. the *Antennae* (a structure that appears more like a non-collimated outflow originating from the galaxy-wide star-formation, rather than a galactic wind-type outflow). One might have expected the NGC520 wind structures to distort very quickly, due to the rapid evolution and violence of the environment. However, the structure appears, especially towards the centre, to be rather classical in nature, and a single starburst-produced wind might indeed last intact for some time during a major interaction.

- 15 X-ray sources are detected within the optical confines of the system. Of these, 3 or possibly 4 are ULXs, each with L_X (0.2–10 keV) $\gtrsim 10^{39}$ erg s $^{-1}$. One of the ULXs lies at the primary nucleus, at the centre of the diffuse wind structure, and coincident with the bright radio source at the centre of the molecular disk. A number of the other bright sources are seen to lie near the edge of this molecular disk, in an interface region between the progenitor-galaxy-driven centrally-located neutral ISM and the merger-driven outlying ionised ISM. Significantly, no sources are detected at the secondary nucleus, though within the system, much apparent point-source variability is seen between the observations described here and earlier *ROSAT* observations.

- The slope of the source X-ray luminosity function (XLF) is very flat, due predominantly to the ULXs, and appears in sharp contrast to that of other normal and starburst galaxies. It is however, similar to that of the *Antennae* and other merging galaxies.

- There is much in the X-ray data to support the idea, as suggested by previous multi-wavelength studies, that

NGC520 is the result of an encounter between one gas-rich disk and one gas-poor disk: The number of ULXs observed is only 3–4, while one would expect, on the basis of the FIR luminosity, a number closer to 10. Similarly, L_{ULX} is lower than would be expected, based on the L_{FIR} value. No sources are seen coincident with the secondary (NW) nucleus, nor is any diffuse emission observed in or around this nucleus. The total X-ray luminosity compared to other multiwavelength luminosities, and the diffuse gas fraction are down by about a factor of 2, based on what would be expected, given NGC520’s evolutionary merger stage. It does seem therefore, that, in terms of the X-ray properties, because of the fact that NGC520’s progenitors are likely only one gas-rich disk plus one gas-poor disk, we are observing only ‘half a merger’ when compared with similar gas-rich–gas-rich merger systems, such as the *Antennae* and the *Mice*.

ACKNOWLEDGEMENTS

AMR acknowledges the support of PPARC funding, and thanks the referee (A. Zezas) for very useful comments which have helped to improve the paper.

REFERENCES

- Arp H.C., Madore B.F., 1987, A Catalogue of Southern Peculiar Galaxies and Associations (Cambridge Univ. Press)
- Barnes J.E., 1988, ApJ, 331, 699
- Bernlöhr K., 1993, A&A, 270, 20
- Beswick R.J., Pedlar A., Clemens M.S., Alexander P., 2003, MNRAS, 346, 424
- Brassington N.J., Read A.M., Ponman T.J., submitted to MNRAS
- Colbert E., Heckman T., Ptak A., Strickland D., 2003, astro-ph/0305476
- Condon J.J., Condon M.E., Gisler G., Puschell J.J., 1982, ApJ, 252, 102
- Condon J.J., Helou G., Sanders D.B., Soifer B.T., 1990, ApJS, 73, 359
- Crawford D.F., Jauncey D.L., Murdoch H.S., 1970, ApJ, 162, 405
- Devereux N.A., Eales S.A., 1989, ApJ, 340, 708
- Fabbiano, G., Zezas, A. Murray, S.S., 2001, ApJ, 554, 1035
- Hibbard J.E., van Gorkom J.H., 1996, AJ, 111, 655
- Read A.M., 2003, MNRAS, 342, 715
- Read A.M., Ponman T.J., 1995, MNRAS, 276, 1327
- Read A.M., Ponman T.J., D.K., Strickland D.K., 1997, MNRAS, 286, 626
- Read A.M., Ponman T.J., 1998, MNRAS, 297, 143 (RP98)
- Roberts T.P., Warwick R.S., Ward M.J., Murray S.S., 2002, MNRAS, 337, 677
- Rosati P. et al., 2002, ApJ, 566, 667

- Sanders D.B., Scoville N.Z., Sargent A.I., Soifer B.T., 1988, *ApJ*, 324, L55
- Stanford S.A., 1991, *ApJ*, 381, 409
- Stanford S.A., Balcells 1990, *ApJ*, 355, 59
- Stanford S.A., Balcells M., 1991, *ApJ*, 370, 118
- Stevens I.R., Read A.M., Bravo-Guerrero J., *MNRAS*, 343, L47
- Stockton A., Bertola F., 1980, *ApJ*, 235, 37
- Strickland D.K., Heckman T.M., Weaver K.A., Hoopes C.G., Dahlem M., 2002, *ApJ*, 568, 689
- Swartz A.S., Ghosh K.K., Tennant A.F., Wu K., 2004, *astr-ph/0405498*
- Toomre A., 1977, in *Evolution of Galaxies and Stellar Populations*, Ed. B.M.Tinsley, R.B.Larson, p.401, (New Haven: Yale University Observatory)
- Toomre A., Toomre J., 1972, *ApJ*, 178, 623
- Tovmasyan H.M., Sramek R.A., 1976, *Afz*, 12, 21
- Tully R.B., 1988, *Nearby Galaxies Catalog*. Cambridge University Press, Cambridge
- Yun M.S., Hibbard J.E., 2001, *ApJ*, 550, 104
- Zezas A., Fabbiano G., 2002, *ApJ*, 577, 726